Earth Planets Space, **58**, 113–119, 2006

Aftershock distribution of the 26 December 2004 Sumatra-Andaman earthquake from ocean bottom seismographic observation

Eiichiro Araki[1], Masanao Shinohara[2], Koichiro Obana[1], Tomoaki Yamada[2], Yoshiyuki Kaneda[1], Toshihiko Kanazawa[2], and Kiyoshi Suyehiro[1]

[1]*IFREE, Japan Agency for Marine-Earth Science and Technology, 2-15 Natsushima-cho, Yokosuka, Kanagawa 237-0061, Japan*
[2]*Earthquake Research Institute, the University of Tokyo, 1-1-1 Yayoi, Bunkyo-ku, Tokyo 113-0032, Japan*

(Received July 22, 2005; Revised December 2, 2005; Accepted December 3, 2005; Online published February 17, 2006)

We deployed an OBS network in February–March 2005 in the rupture area of the Sumatra Andaman earthquake on 26 December 2004. We placed 17 short-term OBSs and two long-term OBSs, and recovered OBSs after observation for 19–22 days. The hypocenter distribution from 10-day data of 17 OBS revealed the detailed structure of aftershock seismicity offshore of Sumatra Island. Aftershock seismicity associated with the subducting slab starts 40 km inward from the Sunda trench axis; it ceases at 50 km depth beneath the Aceh Basin, approximately 240 km inward from the trench axis. Aftershocks in 120–170 km from the trench axis consist of a surface with a dip of 10–12° dominated by a dip-extension type mechanism. Beyond the southwestern edge of the Aceh Basin, the aftershock activity becomes higher, and dominated by dip-slip type earthquakes, with a slightly increased dipping angle of 15–20°. Three along-arc bands of shallow seismicity were identified at 70 km inward from the Sumatra trench, 110 km inward from the trench, and in the south of the Aceh Basin. These locations correspond to steep topographic slopes in the accretionary prism, suggesting the present evolutional activity of the accretionary prism offshore Sumatra Island.

Key words: Sumatra, Andaman, aftershock, seismicity, ocean bottom seismograph (OBS), accretionary prism, plate boundary.

1. Introduction

The Sumatra-Andaman earthquake of 26 December 2004 revealed an historically large seismic moment released beneath the seafloor 1200 km from offshore Simeulue Island south of Sumatra Island to the north of Andaman Island. That seismic moment engendered a devastating tsunami that killed more than 300,000 people. The earthquake has been analyzed extensively using various seismo-geodetic means such as teleseismic body waves (Ji, 2005; Yagi, 2005; Yamanaka, 2005), earth's free oscillation (Stein and Okal, 2005), and tsunami observed using satellite altimetry (Hirata *et al*., 2005). All analyses above are based on observed data that were taken remotely from the rupture area. With such observed data, it is difficult to infer the precise geometry of the earthquake faults that slipped during the earthquake. Many of those analyses subsumed the geometry of a plate boundary in which the rupture took place. They relied on results of Harvard CMT analyses or geometry of background seismicity. The former assumes that the entire rupture took place in a simple planar surface. The latter data (from such a catalog as Engdahl *et al*., 1998) has great limitations that are unavoidable from the scarce number of earthquakes observed during 40 years or so. It is especially difficult above 30 km to find an appropriate depth and dipping angle of the plate interface from the seismicity.

Therefore, it is of great importance to observe seismic activity closely soon after a large earthquake to unveil the geometry and dynamics of the subducting plate in and around the rupture area. According to the Omori relation of aftershocks, aftershock activity will decay quickly with time. In Sumatra Island, the destructive damage of infrastructure due to the devastating tsunami made it difficult to install seismographic networks for aftershock survey. The depth accuracy of offshore seismic activity analyses from existing land data was very limited. Because of those limitations, we decided to bring a research vessel into the rupture area quickly to install a seismographic network of ocean bottom seismographs (OBSs).

After the Sumatra-Andaman earthquake on 26 December 2004, seismic observation using OBSs was carried out in the offshore northern part of the Sumatra Island, where a large co-seismic slip was inferred from teleseismic analyses. We laid an OBS network to determine the detail of aftershock seismicity. Purposes of this OBS observation are to determine the precise location of aftershocks around the area of the main shock. The precise image of aftershocks as well as those mechanisms should help us to delineate the geometry of the subducting oceanic plate that caused the Sumatra-Andaman earthquake, as well to assess possibilities for large aftershocks by recovery of subsurface faults.

2. OBS Network and Data

In all, 17 short-term OBSs from Japan Agency for Marine Earth-Science and Technology (JAMSTEC) and Earth-

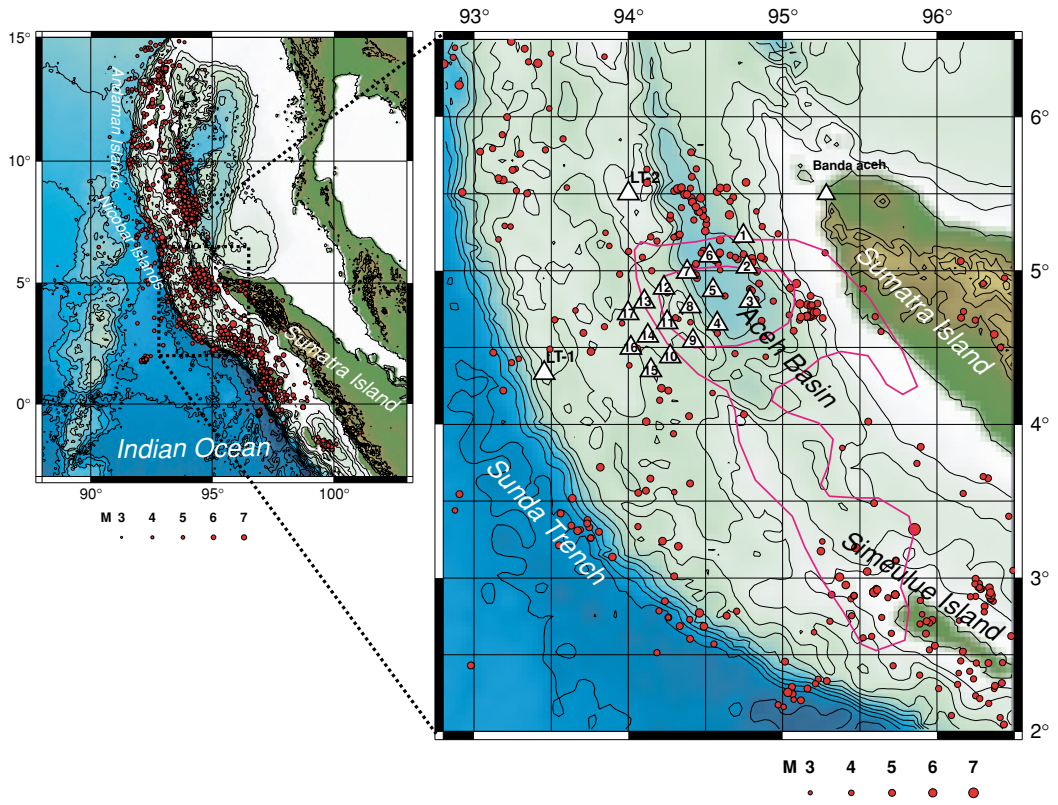

Fig. 1. Location map of OBSs. The OBSs are represented as triangles with station names. OBSs 1–17 were recovered in the NT05-08 cruise for this study. LT-1 and LT-2 are the long-term OBSs. Banda Aceh station is a land seismic station maintained by the Meteorological and Geophysical Agency of Indonesia (BMG). Aftershocks from PDE catalog by USGS during 12/26/2004–4/17/2005 are plotted as red circles scaled by magnitude, as indicated at the bottom. Sizes of circles correspond to the reported magnitude. Purple contours show a slip distribution of the 26 December earthquake after Yagi (2005).

quake Research Institute, the University of Tokyo (ERI) as well as two long-term OBSs from ERI were deployed (Fig. 1) during the R/V Natsushima NT05-08 cruise of JAMSTEC.

The along-arc coverage of the deployed OBS network is approximately 50 km. That coverage was restricted by the number of the available OBSs and the spacing required for precise determination of earthquake depths. Distances between stations were made shorter to the Sumatra trench. Such variable station-to-station distances were intended to better resolve depths of aftershocks in the subducting slab, and yet to offer wider network coverage with a limited number of OBSs. Distances are adjusted to be similar to the depth of the subducting plate boundary assumed from the seismicity catalog by Engdahl *et al*. (1998). The OBSs are aligned as three parallel arrays in 55° of north, parallel to the dipping direction of the Wadati-Benioff zone.

The area of the short-term OBS network covers the area of seaward transition about 100 km to the Sumatra trench from a very large slip area in the main shock determined by Yagi (2005), as shown by contours in Fig. 1. The network location also corresponds to the area of large seafloor deformation inferred from tsunami waveform inversion by Hirata *et al*. (2005). The landward edge of the network is situated at the high aftershock activity area found from globally determined seismicity (PDE) by the United States Geological Survey. Using such seismicity data, the known aftershocks become few to the southwest of the network, although some were of indeterminate depth.

During the cruise, we recovered all 17 short-term OBSs. The observation period of the short-term OBSs was 20 February–13 March 2005 (19–22 days). One of the 17 OBSs did not start recording in the seafloor, but the remainder of the OBSs recorded good three-component seismograms. After observation until the end of July 2005, we recovered one of the long-term OBSs by R/V Baruna Jaya I-BPPT (Agency for the Assessment and Application of Technology, Indonesia). In all, we analyzed seismic data from the 17 OBSs deployed offshore of Sumatra Island. In each OBS record, more than 200 events were discernible as a daily average. In some OBSs (9, 11, 12, 14, 15, 16, 17 in Fig. 1), periods of high noise occurred one or two times daily. Sites of the periodic high noise were situated in the shallower seafloor in outer-arc high mountains, implying that the seafloor tidal current was high in these locations. The tidal current in such a location was probably higher than on the flat seafloor such as at the bottom of the Aceh Basin.

3. Analysis

We identified earthquakes by comparing short-term and long-term averages of OBS records in the 4–15 Hz pass band. We identified events that were apparent at more than three OBS stations. Hypocenters were determined for the events identified from the OBS data from 20 February–1 March. We also examined events located by USGS

Table 1. Summary of travel time residuals and station correction. For each OBS, mean (O-C) and the root-mean-square residual (RMS) of the model to observation for P and S readings are listed along with station correction (P SC and S SC, respectively).

station	P(O-C)	P(RMS)	S(O-C)	S(RMS)	P SC(s)	S SC(s)
OBS02	−0.041	0.221	0.020	0.669	0.142	−0.931
OBS03	−0.005	0.214	0.060	0.572	0.037	−1.061
OBS04	0.035	0.247	0.121	0.718	−0.289	−2.396
OBS05	0.025	0.369	0.115	0.424	0.200	−0.902
OBS06	−0.021	0.268	0.043	0.563	0.276	−0.807
OBS07	0.008	0.258	0.078	0.489	−0.195	−1.736
OBS08	0.034	0.305	0.141	0.614	0.450	−0.463
OBS09	0.033	0.419	0.101	0.842	0.732	0.383
OBS10	0.018	0.363	0.074	0.945	−0.348	−0.955
OBS11	0.035	0.424	0.105	0.889	0.039	−0.498
OBS12	0.032	0.292	0.094	0.638	0.329	−0.598
OBS13	0.036	0.364	0.127	0.709	−0.234	−0.746
OBS14	0.037	0.325	0.110	0.679	−0.349	−1.225
OBS15	0.018	0.429	0.073	0.744	−0.603	−1.176
OBS16	0.040	0.375	0.102	0.840	−0.299	−0.999
OBS17	0.029	0.414	0.107	0.760	−0.338	−1.031
LT-1	−0.004	0.136	−0.012	0.925	0.000	−0.961

throughout the OBS observation period from 20 February–11 March to calibrate the hypocenter of globally determined earthquakes.

Location of earthquakes was performed using the maximum likelihood method by Hirata and Matsu'ura (1987) in a 1-D velocity model. Both P and S arrival picks were used in analyses. In results presented hereafter, we chose events that were located with accuracy of better than 10 km for both horizontal and depth.

There was no detailed known seismic structure in the area of the OBS network. The seismic velocity structure for the hypocenter determination was assumed as Fig. 2. Above 30 km depth, we assumed a structure similar to that offshore of Sumatra Island (SO138-03 in Kopp *et al.*, 2001) further south of our observation area. Below 37 km depth, the P-wave velocity is similar to that of Kennett and Engdahl (1991). We assumed $Vp/Vs = \sqrt{3}$ for the entire model. After locating earthquakes, we inspected dependence of their traveltime misfit on epicentral distance for each OBS. No marked dependence was apparent except for OBS 8 and OBS 9 (Fig. 1), which had positive O-C, and OBS 15 and OBS 16, which had negative O-C for larger epicentral distances. Even for these stations, the average deviation from our model is less than one second.

We applied station correction to P-phase and S-phase readings to take account of the effects of sediment cover and shallow structure that differ from station to station. The correction was obtained for each OBS by the average of the travel time differences of observation from those calculated for our structural model. After correction, the averaged difference between observations and calculations (Table 1) fell to within 0.05 s for P-phases and 0.15 s for S-phases. The root mean square (rms) value of the misfit became less than 0.5 s and 1.0 s, respectively, for P-phases and S-phases.

Magnitudes of these earthquakes were evaluated using the duration of seismic waves for each event, which is similar to the method of Tsumura (1967). For events reported by USGS, we compared the estimated duration magnitude (Mf-p) with the reported body-wave magnitude (MB). The relation between Mf-p and MB showed a scattered distribution. We adjusted the equation for duration magnitude to match Mf-p to the MB for events of MB $\sim$ 4.6, giving Mf-p $= -1.74 + 2.85\log$(F-P), where F-P is the event duration in seconds.

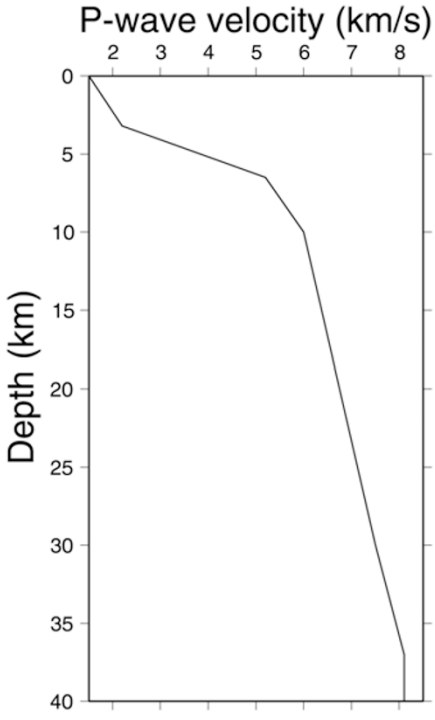

Fig. 2. A P-wave seismic velocity model is assumed in the hypocenter determination in this study.

We also inspected polarity of the P-wave first motion of vertical component to assess earthquake mechanisms. The amount of observed polarity from 16 OBSs was insufficient to determine focal mechanisms for each event. In most cases, we were able to read only several or more first motion polarity. Therefore, we combined observed polarity data for events of similar location to find representative focal mechanism for the group of earthquakes.

4. Results

During 20 February–1 March, 1098 events were located using OBS observation. As shown in Table 2, 17 events were relocated from the USGS PDE catalog between 21 February and 11 March. All located earthquakes, with accuracy of better than 10 km for both horizontal and depth, are displayed in Fig. 3. All globally determined earthquakes were relocated along the dipping plate that subducted from the Indian Ocean. Some events were relocated with a shift of as much as 50 km horizontally and 25 km in depth.

The magnitudes of earthquakes determined by OBSs during the period of 20 February–1 March were distributed from -0.5 to 5. All events of magnitude (M) greater than 1.5 beneath the OBS network were addressed by our analysis, as suggested from the frequency-magnitude distribution of the located earthquakes.

5. Discussion

Most events were located with a dip delineating a subducting plate from the Sunda trench towards Sumatra Island. The area of aftershock seismicity starts at approximately 40 km from the Sunda trench axis, as defined by the deepest point of the seafloor. Aftershocks extend for 200 km northeast in the trench orthogonal direction. Fewer earthquakes were located in the upper plate.

Depths of seismicity along the subducting slab were not well determined near the Sunda Trench, but are at least shallower than 30 km. The dip angle of seismicity in the subducting plate would be shallower than 10° to a point 120 km from the trench, but the depth of seismicity is ambiguous. Beneath the OBS network, where the depth of seismicity was better determined, the slab seismicity concentrates in an approximately 10-km-thick plate. From 120 km from the trench axis, slab seismicity continues with a dip angle of approximately 10–12° to the southwestern edge of Aceh Basin (as index C of Fig. 4) at 25 km depth. The dip angle is slightly deeper than that of the Harvard quick CMT solution of the 26 December event (8°), and similar to those assumed by Ji (2005) (11°), Yagi (2005), and Hirata *et al.* (2005) (10°). The focal mechanism of this seismicity as a whole is a down-dip extension type mechanism (Fig. 4).

Seismicity along the subducting slab in the survey area is characterized in two domains in the trench normal direction divided around the southwestern edge of the Aceh Basin. Beneath the Aceh Basin, dipping slab seismicity becomes more active; in addition, their mechanism changes (beyond the index C in Fig. 4). Transition of the activity is prominent and sudden. The dipping angle of the seismicity seems also to increase to 15–20°, corresponding to this transition. Their focal mechanism changes from a down-dip extension to dip-slip type, as revealed from the dip of planar seismicity and nodal angle of the focal mechanism. The dip-slip aftershocks in this area are concentrated in relatively small patches. A small number of upper plate earthquakes are identifiable: they make a branch from the subducting plate interface towards the south of the Aceh Basin. The area of high inter-plate seismicity starts from 25 km depth and ceases at 50 km depth at the northern edge of Aceh Basin. Dip-slip aftershocks might suggest an ongoing post-seismic slip at the plate interface beneath the Aceh Basin.

The focal mechanism of the main shock of 26 December 2004 is known to be low-angle dip slip type from seismic moment analysis. Teleseismic analyses (Yamanaka, 2005; Ji, 2005) suggest co-seismic slip of 2–6 meters in the area between B and C (Fig. 4) during the December main shock. Tsunami analysis (Hirata *et al.*, 2005) also infers large co-seismic slip in this area. These analyses indicate that the plate boundary of this area should have slipped during the main shock. However, we now see very inactive dip-slip seismicity in the area. Lack of aftershocks suggests complete strain release during the main shock, and possibly little after-slip occurrence.

The composite focal mechanism of the aftershock suggests that the subducting slab above 25 km depth is probably under tension, possibly because of slab pull from the subducting plate at deeper depth between regions C and D. In the future, it will be interesting to observe temporal changes of focal mechanisms and activity in this area. The change of the aftershock focal mechanism might indicate a stress change of the subducting plate in the process of possible postseismic slip and recovery. In this sense, continuous OBS deployments off Sumatra Island, as well as other geodetic measurements such as those using GPS, will greatly benefit our understanding of postseismic processes of large earthquakes.

Almost no aftershocks occur in the subducting slab below Sumatra Island beyond a depth of 50 km (D in Fig. 4), whereas some earthquakes were seen well beyond that depth in the background seismicity (Engdahl *et al.*, 1998). Analyses of our 10-day OBS data showed that there was also no shallow seismicity in Sumatra Island.

Distribution of upper plate seismicity was concentrated in three band areas along the Sumatra arc: 1) 70 km from the trench, where the seafloor becomes shallower to 2000 m; 2) in the middle of outer-arc high, approximately 110 km from the trench axis; and 3) at the southern edge of Aceh Basin, approximately 170 km from the trench. These three areas have clear correspondence with steep slopes in seafloor topography, as indicated by indexes A–C in Fig. 4. These zones of shallow seismicity might be associated with splay faults.

Correspondence of the upper plate seismicity with the steep topographic slope probably reflects activity of the accretionary prism in the area. At the southern edge of Aceh Basin (C in Fig. 4), the West Andaman Fault is suggested to connect to the Mentawai Fault north of the Simeulue Island (Diament *et al.*, 1992). We observed much higher seismicity in the middle of the outer-arc high (B) and near the Sunda trench (A) than around the suggested West Andaman fault (C). This discrepancy might suggest existence of another fault system in the outer-arc high that is more active

Table 2. List of earthquakes relocated by OBS network. Earthquakes are from PDE catalog by USGS. For each event, origin time, latitude, longitude, depth and magnitude of both OBS relocation and of PDE catalog are listed. The magnitude scale of OBS relocation is duration magnitude (Mf-p).

OBS					USGS PDE				
Date/Time	Latitude (°)	Longitude (°)	Depth (km)	Mf-p	Time	Latitude (°)	Longitude (°)	Depth (km)	Magnitude
2005/02/21 20:18:38.618	5.44546	94.34340	44.08	4.4	20:18:38.00	5.417	94.432	30	4.2 MB
2005/02/21 21:08:57.599	5.16624	94.71945	50.43	3.6	21:08:54.95	4.975	94.442	30	4.3 MB
2005/02/21 23:19:37.650	4.95412	94.35669	33.68	4.9	23:19:36.36	5.025	94.426	30	4.5 MB
2005/02/22 00:10:09.315	5.72749	94.38088	48.52	4.9	00:10:09.28	5.536	94.403	30	4.6 MB
2005/02/23 00:19:59.610	3.92818	94.36303	49.76	4.2	00:19:59.18	3.939	94.293	31.4	4.4 MB
2005/02/23 18:24:42.237	4.61391	95.19237	47.13	5.1	18:24:39.74	4.707	95.178	30	4.9 MB
2005/02/25 01:18:29.088	4.30539	93.85451	15.25	3.5	01:18:31.88	4.384	94.005	46.5	4.3 MB
2005/02/25 15:03:20.088	5.22280	94.78230	54.52	4.2	15:03:18.58	5.385	94.830	30	4.3 MB
2005/02/26 07:10:57.679	4.72867	94.83299	40.74	4.6	07:10:54.81	4.592	94.577	30	4.4 MB
2005/02/27 04:08:36.237	5.07417	93.17958	13.49	3.4	04:08:37.63	5.286	93.237	30	4.3 MB
2005/02/27 09:00:45.409	5.09790	94.50416	46.40	4.9	09:00:45.02	5.114	94.472	30	4.6 MB
2005/02/28 09:26:28.922	5.46769	94.47711	45.31	4.7	09:26:28.60	5.216	94.294	47.9	4.7 MB
2005/03/01 19:22:40.872	5.46682	94.27490	31.28	4.9	19:22:43.88	5.410	94.344	53.7	4.7 MB
2005/03/02 14:45:35.042	5.30233	94.37879	39.63	5.3	14:45:33.28	5.224	94.316	30	4.9 MB
2005/03/03 13:41:31.663	4.70456	93.71197	20.91	3.6	13:41:31.63	4.742	93.658	30	4.2 MB
2005/03/03 14:45:38.354	5.59328	94.37762	50.36	4.5	14:45:35.69	5.220	94.144	30	4.8 MB
2005/03/11 09:51:46.934	5.17901	94.75065	54.40	4.5	09:51:44.60	4.952	94.444	30	4.9 MB

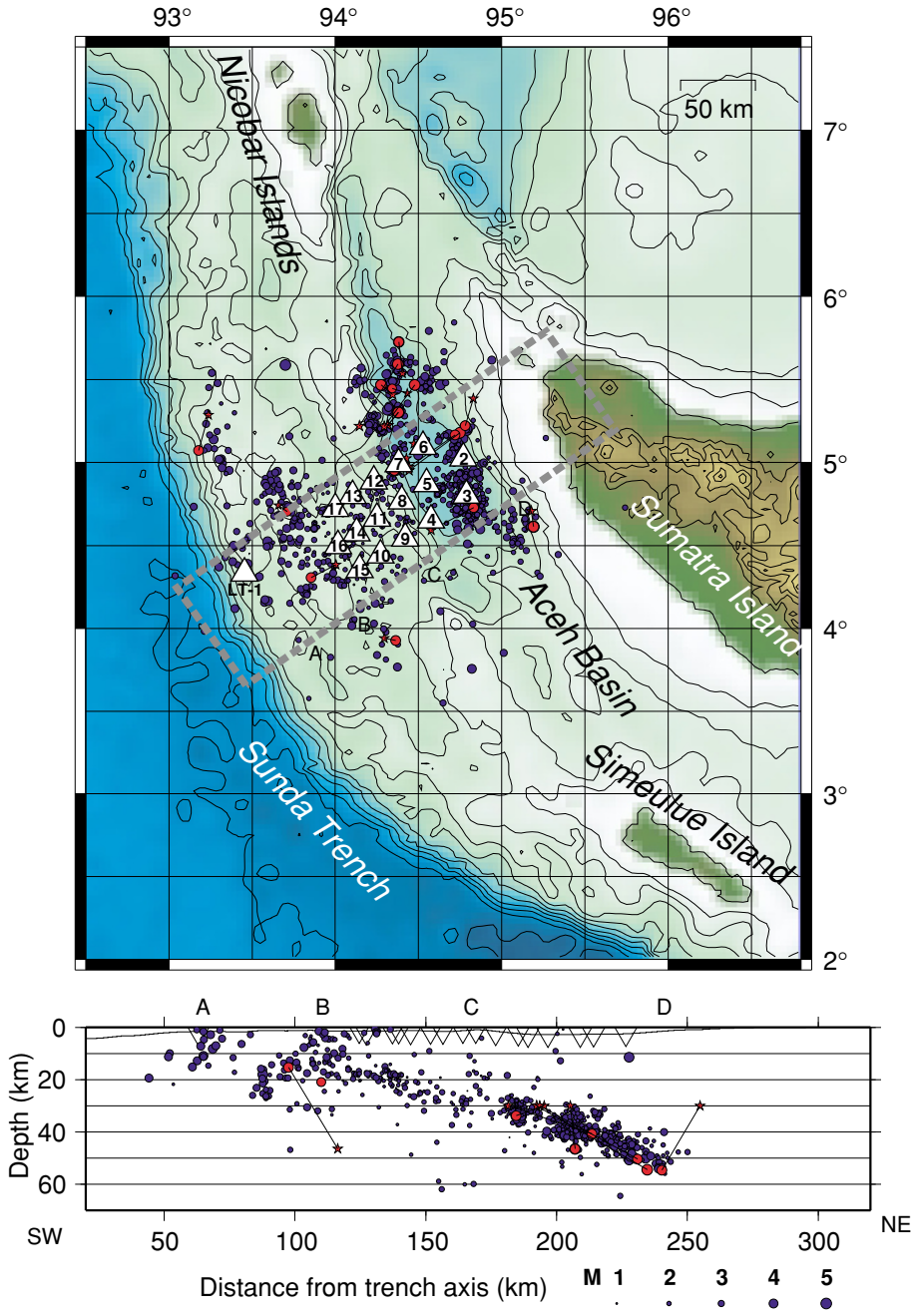

Fig. 3. Seismicity determined from the OBS data of 10-days from 20 February–1 March are shown as blue circles. The circles are scaled according to their duration magnitude (Mf-p) as the bottom scale. The OBS relocated earthquakes from the USGS PDE catalog between 21 February and 11 March are indicated as red circles. Their PDE locations are indicated as red stars. The OBS locations used for hypocenter determination are shown as triangles with their station names. The bottom plate is a cross sectional projection of the hypocenter inside that shown by a dashed box in the map, with horizontal scale showing distance from the Sunda trench. The azimuth of the projection plane is 55° from the north. Seafloor topography and OBS locations (inverse triangles) are also shown. Indexes A-D in the cross section are also shown in the map.

than the West Andaman fault. We require better seafloor topography data to better understand active faults in this area. The focal mechanism of the shallow seismicity in the accretionary prism is important information to discuss its evolution, but it cannot be determined clearly using the present analysis.

6. Conclusions

We deployed the OBS network in February–March 2005, within two months after the devastating Sumatra-Andaman earthquake of 26 December 2004. The OBS network was designed to situate above the area of maximum slip in the earthquake that generated the historical tsunami in the Indian Ocean. We deployed 17 short-term OBS and two long-term OBSs. Short-term OBSs were recovered during the same cruise of deployment by R/V Natsushima after observation for 19–22 days, whereas the long-term OBSs continued observation until the end of July 2005.

The hypocenter distribution from 10-day data of 17 OBS was sufficient to delineate a detailed structure of aftershock seismicity occurring offshore of Sumatra Island. Aftershock seismicity associated with the subducting slab starts

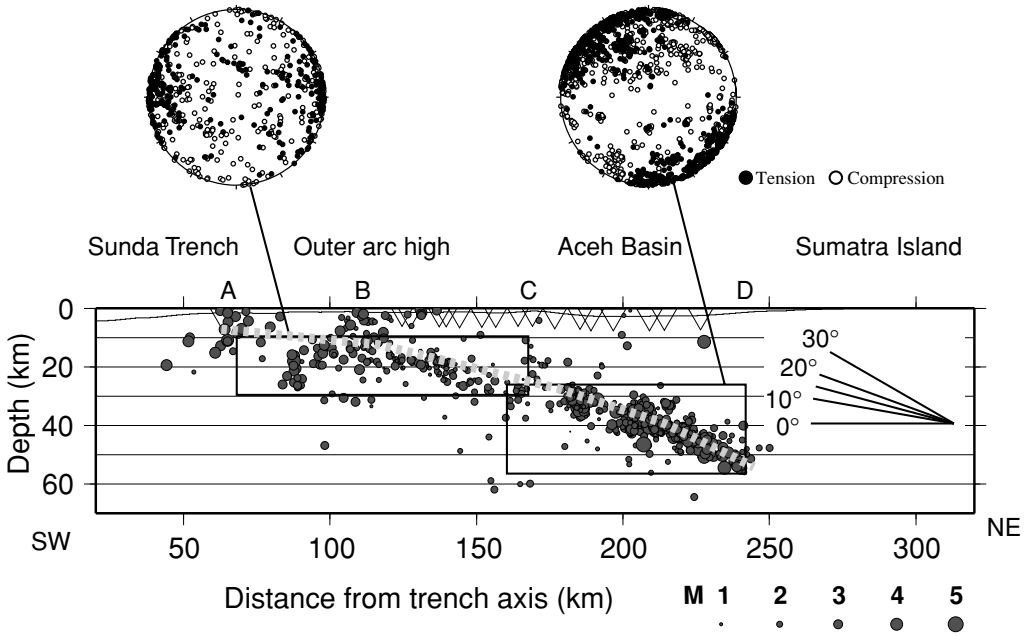

Fig. 4. Illustrated cross section seismicity, as shown by Fig. 3. Dashed gray lines indicate the plate boundary and possible splay faults estimated from OBS seismicity. Composite focal mechanisms are inferred from P-wave first motion polarity plots above. The P-wave vertical motion polarity data, of which earthquakes are in the solid boxes, are projected into the same cross-sectional plane, as shown by black circles (tension or up), white circles (compression or down). The projected areas are divided by indexes A–D, which correspond to 70 km from the Sunda Trench (A), the middle mountain of the outer-arc high (B), the Aceh Basin's southwestern edge, (C) and the downdip limit of the aftershock seismicity, (D) in the south of Sumatra Island. The southwestern edge of the profile corresponds to approximately 20 km from the trench axis.

40 km from the Sunda trench axis ceases at 50 km depth beneath the Aceh Basin approximately 240 km inward from the trench axis. To the point 120 km from the trench axis, the dip angle of the subducting plate is shallower than 10°. Beneath the OBS network, most of the aftershocks were confined to within a 10-km-thick surface dipping landward. In 120–170 km from the trench axis, aftershocks consist of a surface with a dip of 10–12°, and are dominated by a dip-extension type mechanism. Beyond the point collocated with the southwestern edge of the Aceh Basin, the aftershock activity becomes higher, and their focal mechanisms are dominated by dip-slip type earthquakes, with a slightly increased dipping angle of 15–20°. These dip-slip aftershocks might suggest occurrence of a post-seismic slip beneath the Aceh Basin.

The OBS observation identified three along-arc bands of shallow seismicity in the upper plate: 70 km from the Sunda trench, 110 km inward from the trench, and in the south of the Aceh Basin. Existence of splay faults is inferred in the shallow seismicity areas corresponding also to steep topographic slopes in the accretionary prism, suggesting that the present evolution of the accretionary prism was activated by large earthquakes offshore Sumatra Island.

Acknowledgments. We express our deep appreciation to Captain Fusao Saito, officers and crew of R/V Natsushima for their professional operations that enabled us to make our observations. Operation of OBS deployment and recovery by onboard technicians from Nippon Marine Enterprise, Ltd. was an indispensable part of our scientific research. We appreciate all the onboard scientific party of the NT05-08 Natsushima cruise for their constructive discussion during and after the cruise. Figures were partially prepared using GMT (Wessel and Smith, 1998). This research is supported by special coordination funds for promoting science and technology from the Ministry of Education, Culture, Sports, Science and Technology (MEXT), Japan.

References

Diament, M., H. Harjono, K. Karta, C. Deplus, D. Dahrin, M. T. Zen, Jr., M. Gerard, O. Lassal, A. Martin, and J. Malod, Mentawai fault zone off Sumatra: A new key to the geodynamics of western Indonesia, *Geology*, **20**, 259–262, 1992.

Engdhal, E., R. van der Hilst, and R. Buland, Global teleseismic earthquake relocation with improved travel times and procedures for depth determination, *Bull. Seismol. Soc. Am.*, **88**, 722–743, 1998.

Hirata, K., K. Satake, Y. Tanioka, T. Kuragano, Y. Hasegawa, Y. Hayashi, and N. Hamada, The 2004 Indian Ocean Tsunami: Tsunami Source Model from Satellite Altimetry, *Proceedings of 22nd International Tsunami Symposium*, Chania, Crete Isl., Greece, 27–29 June, 2005.

Hirata, N. and M. Matsu'ura, *Phys. Earth Planet. Inter.*, **47**, 50–61, 1987.

Ji, C., Preliminary Result of the 04/12/26 (Mw 9.0), Off W. Coast of Northern Sumatra Earthquake, 2005. http://www.gps.caltech.edu/_jichen/Earthquake/2004/aceh/aceh.html

Kennett, B. L. N. and E. R. Engdahl, Traveltimes for global earthquake location and phase identification, *Geophys. J. Int.*, **105**, 429–465, 1991.

Kopp, H., E. R. Flueh, D. Klaeschen, J. Bialas, and C. Reichert, Crustal structure of the central Sunda margin at the onset of oblique subduction, *Geophys. J. Int.*, **147**, 449–474, 2001.

Stein, S. and E. Okal, Speed and size of the Sumatra Earthquake, *Nature*, **434**, 581–2, 2005.

Tsumura, K., Determination of earthquake magnitude from duration of oscillation, *Jishin*, **2**, **20**, 1, 30–40, 1967 (in Japanese).

Wessel, P. and W. H. F. Smith, New, improved version of Generic Mapping Tools released, *EOS Trans. Amer. Geophys. U.*, **79**(47), 579, 1998.

Yagi, Y., Preliminary Results of Rupture Process for 2004 Off Coast of Northern Sumatra Giant Earthquake (ver. 1), http://iisee.kenken.go.jp/staff/yagi/eq/Sumatra2004/Sumatra2004.html, 2005.

Yamanaka, Y., 04/12/26 Off W. Coast of N. Sumatra (revised), EIC Seismological Note: No. 161+, http://www.eri.u-tokyo.ac.jp/sanchu/Seismo_Note/2004/EIC161ea.html, 2005.

E. Araki (e-mail: araki@jamstec.go.jp), M. Shinohara, K. Obana, T. Yamada, Y. Kaneda, T. Kanazawa, and K. Suyehiro